PCP
PLANT & CELL PHYSIOLOGY

Special Issue – Regular Paper

A Three-Dimensional Scanning System for Digital Archiving and Quantitative Evaluation of *Arabidopsis* Plant Architectures

Itsuki Kunita[1], Miyo Terao Morita[2], Masashi Toda[3] and Takumi Higaki[4,*]

[1]Faculty of Engineering, University of the Ryukyus, Senbaru 1, Nishihara-cho, Nakagami-gun, Okinawa 903-0213, Japan
[2]Division of Plant Environmental Responses, National Institute for Basic Biology, Nishigonaka 38, Myodaiji, Okazaki, Aichi 444-8585, Japan
[3]Center for Management of Information Technologies, Kumamoto University, Kurokami 2-39-1, Chuo-ku, Kumamoto 860-8555, Japan
[4]International Research Organization for Advanced Science and Technology, Kumamoto University, Kurokami 2-39-1, Chuo-ku, Kumamoto 860-8555, Japan

*Corresponding author: E-mail, thigaki@kumamoto-u.ac.jp
(Received 14 January 2021; Accepted 21 May 2021)

A plant's architecture contributes to its ability to acquire resources and reduce mechanical load. *Arabidopsis thaliana* is the most common model plant in molecular biology, and there are several mutants and transgenic lines with modified plant architecture regulation, such as *lazy1* mutants, which have reversed angles of lateral branches. Although some phenotyping methods have been used in larger agricultural plants, limited suitable methods are available for three-dimensional reconstruction of *Arabidopsis*, which is smaller and has more uniform surface textures and structures. An inexpensive, easily adopted three-dimensional reconstruction system that can be used for *Arabidopsis* is needed so that researchers can view and quantify morphological changes over time. We developed a three-dimensional reconstruction system for *A. thaliana* using the visual volume intersection method, which uses a fixed camera to capture plant images from multiple directions while the plant slowly rotates. We then developed a script to autogenerate stack images from the obtained input movie and visualized the plant architecture by rendering the output stack image using the general bioimage analysis software. We successfully three-dimensionally and time-sequentially scanned wild-type and *lazy1* mutant *A. thaliana* plants and measured the angles of the lateral branches. This non-contact, non-destructive method requires no specialized equipment and is space efficient, inexpensive and easily adopted by *Arabidopsis* researchers. Consequently, this system will promote three- and four-dimensional phenotyping of this model plant, and it can be used in combination with molecular genetics to further elucidate the molecular mechanisms that regulate *Arabidopsis* architecture.

Keywords: *Arabidopsis* plant architecture • Digital archiving • Quantitative evaluation • Three-dimensional reconstruction • Visual volume intersection method

Introduction

Plants construct a characteristic architecture by extending their branches at certain angles (Wang and Jiao 2018, Nakamasu and Higaki 2019). Plant architecture may contribute to both acquisition of resources such as light and water, and reduction of mechanical load due to the weight of the branches, leaves or snow accumulation. Recent molecular biological studies have revealed genes that regulate plant architecture (Sussex and Kerk 2001, Hill and Hollender 2019), and the need for advanced phenotyping methods for plant architecture is increasing. Although plant architecture can be approximated in two dimensions, it should be analyzed as a three-dimensional structure to accurately elucidate the morphological features. Recent advances in remote sensing technologies, such as light detection and ranging (LIDAR), and image measurement technologies, such as structure from motion (SfM), have stimulated remarkable progress in large-scale three-dimensional analysis of crop rows and tree forests, mainly in agriculture and ecology (Gülci 2019, Qiu et al. 2019). LIDAR is a technique that estimates distances by measuring the time it takes for the reflected energy of an irradiated laser pulse to return to the sensor (Qiu et al. 2019). Alternatively, SfM is a technique that reconstructs three-dimensional structures from numerous images taken from different positions by calculating the camera motion and three-dimensional positions of the object based on the corresponding positions in the images (Gülci 2019). Because the corresponding positions are automatically extracted by image analysis, SfM is more suitable for structures with characteristic patterns or shapes that are easily recognized by computational methods. These technologies have also been applied to three-dimensional analysis of individual agricultural plant bodies such as aubergine (Omasa et al. 2007), tomato (Omasa et al. 2007) and chili (Paturkar et al. 2020). In addition, the visual volume intersection method,

Plant Cell Physiol. 62(12): 1975–1982 (2021) doi:https://doi.org/10.1093/pcp/pcab068, Advance Access publication on 28 June 2021, available online at https://academic.oup.com/pcp

which three-dimensionally reconstructs the objects from object silhouettes in multiple-angle images by intersection of silhouette cones, has been used for three-dimensional analysis of agricultural plants, such as cotton (Paproki et al. 2012), tomato (Golbach et al. 2016), banana (Scharr et al. 2017) and maize (Scharr et al. 2017).

Arabidopsis thaliana, which is the most commonly used plant model in molecular biology, has a thin flower stem with a diameter of less than 1 mm; this is substantially smaller than those of the majority of agricultural plants. In addition, its surface textures and structures are relatively uniform, which makes it difficult to extract feature points for SfM. These features might make its three-dimensional reconstruction difficult. However, there are many *A. thaliana* mutants and transgenic lines with various modified molecular regulators of plant architecture, such as the cell wall (Hongo et al. 2012, Mitsuda et al. 2007, Takenaka et al. 2018), organ straightening (Okamoto et al. 2015) and gravitropic response (Taniguchi et al. 2017). Therefore, the importance of studying *Arabidopsis* plant architecture and associated molecular mechanisms is indisputable. Importantly, three-dimensional phenotyping techniques should be easily understood and operated by *Arabidopsis* researchers; otherwise, the technique will not be used by *Arabidopsis* research communities and will not be able to deepen our basic biological understanding of plant architecture.

In this study, we developed a three-dimensional reconstruction system for *A. thaliana* plants based on the visual volume intersection method, in which a fixed camera captures images of each plant from multiple directions while it rotates at low speed on a rotator. Our system does not require specialized equipment and is relatively inexpensive. It can also be set up in a small space; thus, it can be easily adopted by many laboratories that specialize in plant molecular biology. This non-contact, non-destructive method enables acquisition of three-dimensional information over time by monitoring plant growth. In addition, our system can also be used for quantitative evaluation of morphological changes. We used this system to quantitatively evaluate the morphology of the lateral branches of wild-type (WT) and *lazy1* mutant *A. thaliana*, the latter of which is known to have reversed angles of their lateral branches (Taniguchi et al. 2017). Our system is expected to promote three- and four-dimensional phenotyping of *Arabidopsis* plants.

Results

Multiple-angle imaging system setup

In this study, we focused on the three-dimensional structure of the *A. thaliana* primary inflorescence stem and its branches as a model system for plant architecture. To reconstruct the three-dimensional *Arabidopsis* architecture, we used the visual volume intersection method (Tsai 1987, Laurentini 1994, Kutulakos and Seitz 2000, Cheung et al. 2005), which was previously applied for agricultural plants (Paproki et al. 2012, Golbach et al. 2016, Scharr et al. 2017). In this method, the three-dimensional structures of the object are reconstructed by the intersection of the visual volumes of the multiple-angle images (**Fig. 1**). To obtain multiple-angle images of the standing plant, you can use numerous cameras placed at various angles or move one camera's position in all directions around the plant (**Fig. 1B**). However, this approach would be costly and require extensive equipment for mechanical regulation of camera motion. Therefore, we adopted a system that uses a single camera in a fixed position to capture a movie of an *Arabidopsis* plant rotating at low speed on a rotating table (**Fig. 2A**, **B**).

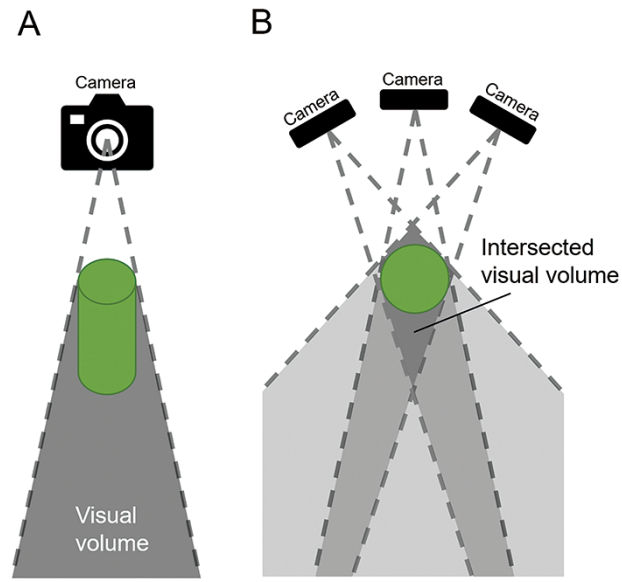

Fig. 1 Visual volume intersection. (A) Visual volume from a single viewpoint. An object can be contained within the visual volume. (B) Intersection of visual volume from three viewpoints. Top view is shown. Object shape can be reconstructed by intersecting the visual volume from multiple angles. It is expected that the accuracy of the three-dimensional reconstruction will improve with increase in the number of images taken from different angles.

To estimate the camera matrix of each captured image, we used a simplified camera matrix estimation method using the calibration target pattern (Baumberg et al. 2005, Datta et al. 2009) (**Fig. 2B**, **C**, 60 red circles) (see also Materials and Methods). To prevent the target pattern from being hidden by the pot, we made a base with a hole in the center so that the pot would be positioned below the target pattern (**Fig. 2A**, **B**). For the target pattern mount, we used a 1.5 cm-thick acrylic plate that was inexpensive and not easily deformed to make the target pattern as flat as possible (**Fig. 2A**, **B**). Additionally, the rosette leaves, rotator and background were covered with black cloth to make it easy to accurately extract the silhouette of the primary inflorescence stem and its branches by image processing (**Fig. 2A**, **B**). Movies of the rotating *Arabidopsis* plant and the target pattern at around 2.5 rpm were acquired with a digital single-lens reflex camera equipped with a single-focus lens (**Fig. 3A**).

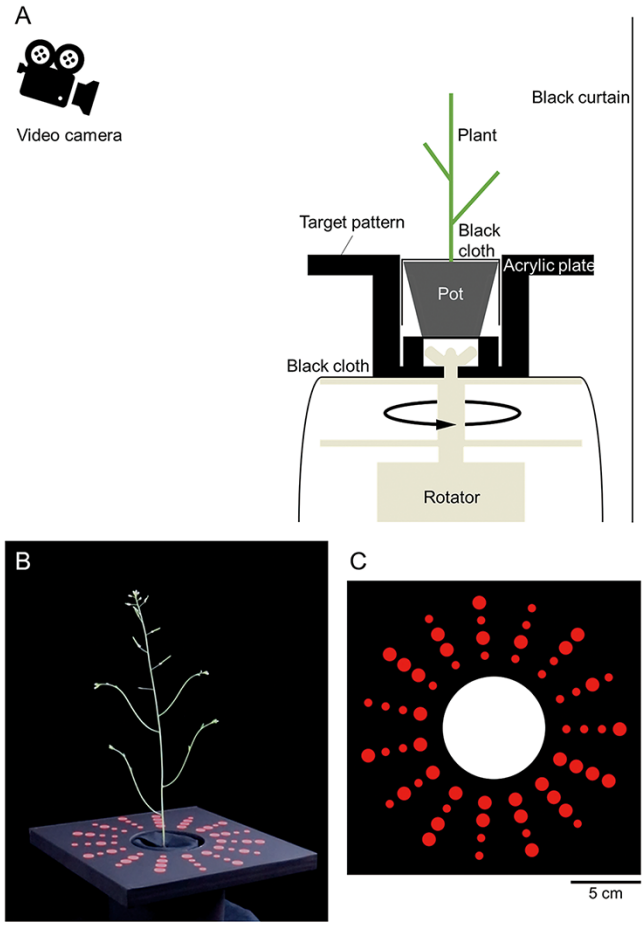

Fig. 2 Multiple-angle imaging system. (A) A schematic illustration of the movie capture system for rotating *Arabidopsis* plants. The plant pot was placed in the center hole of the target pattern so that the target pattern was not hidden by the pot. All objects except for the *Arabidopsis* primary inflorescence stem, branches and the target pattern were covered with a black cloth. (B) Representative image taken by the system. (C) Calibration target pattern used in this study. The pattern was used in previous studies (Baumberg et al. 2005, Datta et al. 2009) but colored red, which is the complementary color of the plant's green.

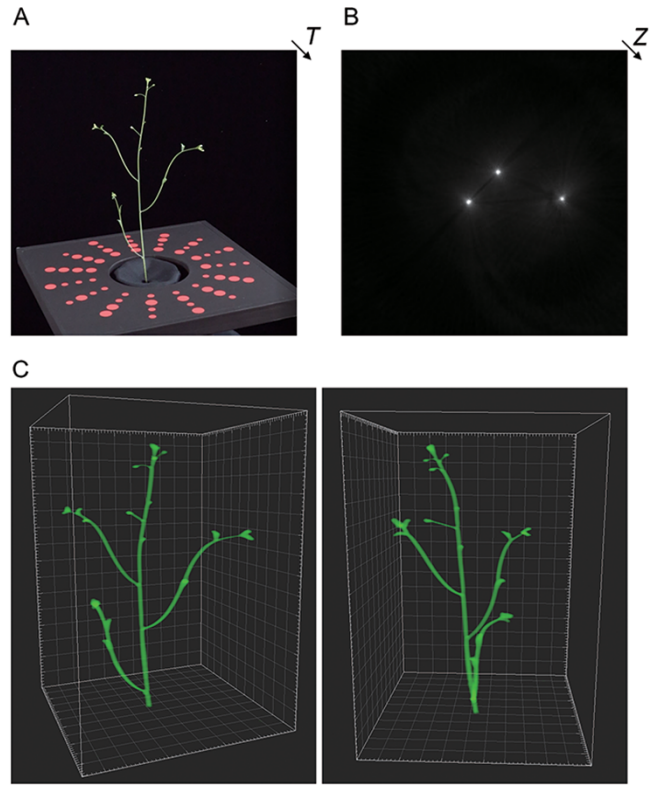

Fig. 3 Three-dimensional reconstruction of *Arabidopsis* architecture. (A) Representative input image. Although the image from a single angle is presented here, approximately 360 images taken in approximately 1° intervals are used for three-dimensional reconstruction. (B) Representative output image of (A). A single frame from the stack image is presented. (C) Volume rendering images of (B). Images from the different viewpoints are shown.

Three-dimensional reconstruction

We developed a script that automatically generated stack images (X–Y–Z images) from the input movie (**Fig. 3A**, **B**) based on the visual volume intersection method (Tsai 1987, Laurentini 1994, Kutulakos and Seitz 2000, Cheung et al. 2005) (see also Materials and Methods). The reconstructed *Arabidopsis* architectures were visualized by rendering of the output stack image using the general bioimage analysis software (e.g. Imaris) (**Fig. 3C**).

In our image analysis framework, the camera matrix of each captured image was first estimated by a simplified camera matrix estimation method using the calibration target (Baumberg et al. 2005, Datta et al. 2009). Specifically, the calibration target plane was set to the X–Y plane of the world coordinate system ($Z = 0$), and the camera matrix was estimated by mapping the world coordinates of the 60 red circular markers drawn on the calibration target to the coordinates of these markers on the image. Next, silhouette images were generated. Then, for each silhouette image, a cone was obtained with the optical center of the camera as the vertex and the silhouette area as the cross section. The object was located within the intersection of the visual volumes of the images as shown in **Fig. 1**. Thus, the circumscribed shape of the object was reconstructed as a three-dimensional image, and the accuracy of the reconstructed shape depended on the number and direction of the analyzed images. The greater the number of images captured from multiple angles, the better the reconstruction accuracy. Finally, the stack images of three-dimensional plant architectures were generated (**Fig. 3B**, **C**).

To examine the relationship between the number of images and the accuracy of three-dimensional reconstruction, we used a sphere model with a 1.5 mm radius formed by a 3D printer (**Supplementary Fig. S1A**). We performed three-dimensional reconstruction of the sphere model and examined the effect of the number of used images on the radius of the reconstructed sphere (**Supplementary Fig. S1B**). The voxel size of the three-dimensional reconstruction was set to 0.01 mm per side. The

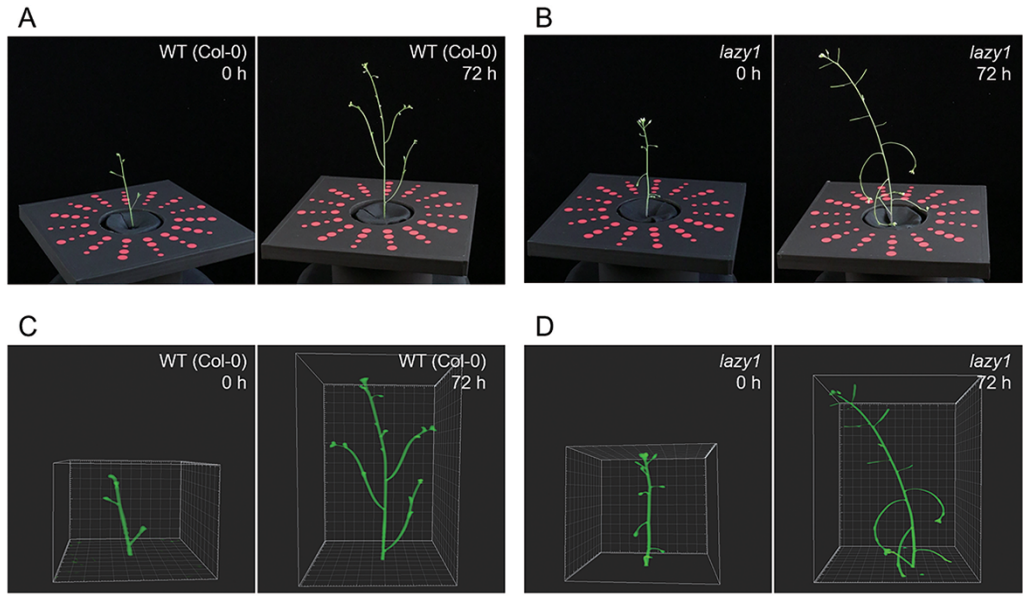

Fig. 4 Three-dimensional digital archiving of the growth in WT and *lazy1* mutant *Arabidopsis*. (A, B) Representative image of the WT Col-0 (0 hours, 39 days old; 72 hours) (A) and *lazy1* mutant (0 hours, 45 days old; 72 hours) plants (B). The plants with a height of around 12 cm were scanned, removed from the rotating table, and then placed back into the growth chamber. The plants were scanned again 72 hours after the first scan. (C, D) Three-dimensional reconstruction images of (A) and (B), respectively.

radius of the sphere of the reconstructed image approached the design value of 1.5 mm and converged after 360 images (**Supplementary Fig. S1B**). With 360 images, the difference between the designed and measured values was approximately −0.001 mm, which was less than the resolution of the analyzed image (approximately 0.05 mm/pixel); this showed that our system can obtain three-dimensional reconstructed images with submillimeter-order and high shape reconstruction accuracy if more than 360 images are analyzed. In this study, we extracted more than 360 images from the 1 minute movie for three-dimensional reconstruction (**Fig. 3A**) (see also Materials and Methods).

Quantitative analyses of lateral branch phenotypes in *lazy1* mutants

The three-dimensional scanning system was applied to quantitatively phenotype the *lazy1* mutant, which is known have reversed angles of lateral branches (**Fig. 4A**, **B**) (Taniguchi et al. 2017). We successfully digitally archived of the growth of WT (Col-0) and *lazy1* mutant plants for 3 days, which demonstrated the utility of our system for four-dimensional phenotyping of *Arabidopsis* plant architectures (**Fig. 4**). The reconstructed time-lapse three-dimensional images were binarized and segmented into the primary inflorescence stem and lateral branches (**Fig. 5A**, **B**, **Supplementary Fig. S2**).

Based on the skeletonized three-dimensional images, the spatial distribution of the angles between the inflorescence stem and lateral branch growth directions was measured (**Fig. 5C**, **Supplementary Fig. S3**). In the WT plants, the branch angles were less than 90°, which indicated that the branches grew against gravity (**Fig. 5C**, WT; **Supplementary Fig. S3**, WT). Additionally, the angle decreased in the basal regions, but gradually reached a plateau toward the branch tip (**Fig. 5C**, WT; **Supplementary Fig. S3**, WT). Alternatively, in the *lazy1* mutant plants, the angles were greater than 90°, which indicated that the branches hang down in the direction of gravity (**Fig. 5C**, *lazy1*; **Supplementary Fig. S3**, *lazy1*). We also observed a tendency of the angle to increase with distance from the tip (**Fig. 5C**, *lazy1*; **Supplementary Fig. S3**, *lazy1*).

In addition, we measured curvatures of the lateral branches based on the skeletonized three-dimensional images (**Fig. 6A**). In the WT plants, decreased curvature was observed in the middle of the branch (**Fig. 6B**, WT), which reflected a loose S-shape of the WT branches. Alternatively, in the *lazy1* mutants, the curvature decrease in the center was not significant, but the curvature increased toward the branch tip (**Fig. 6B**, *lazy1*). Measurement of the average values of the curvature of multiple branches from three WT and three *lazy1* mutant plants revealed that the branches of the *lazy1* mutants were statistically significantly curvier than those of the WT plants ($P = 0.0012$, Mann–Whitney U-tests) (**Fig. 6C**).

Discussion

In this study, we successfully three-dimensionally and time-sequentially scanned *Arabidopsis* architectures with our imaging setup and image analysis techniques. We adopted the visual volume intersection method for three-dimensional reconstruction of the *A. thaliana* primary inflorescence stem and lateral branches (**Fig. 1**). The visual volume intersection method does

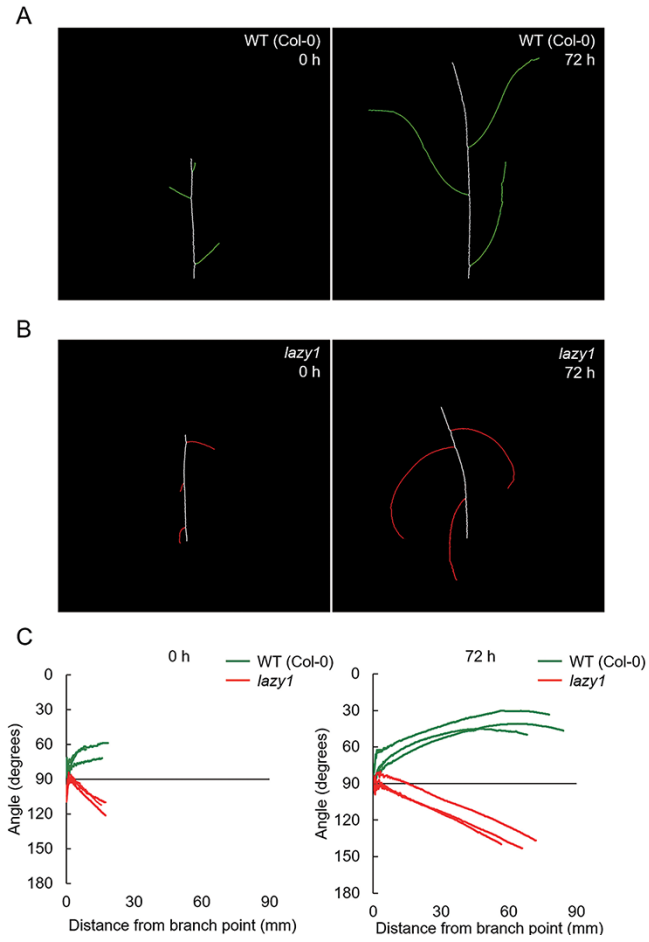

Fig. 5 Measurements of lateral branch angles. (A, B) Three-dimensional images of binarized primary inflorescence stem (white) and lateral branches (color) of the WT Col-0 (0 hours, 39 days old) (A) and *lazy1* mutant (0 hours, 45 days old) plants (B). The original images are shown in Figure 4. (C) Relationship between distance from the branch point and angles between lateral branch and inflorescence stem growth direction. Note that the angles were less than 90° and decreased with distance but gradually plateaued in the WT plant (green), whereas the branch angles were greater than 90° and increased with distance in the *lazy1* mutant (red).

not require expensive equipment and is easy to use. SfM is a similar technique that reconstructs three-dimensional structures from numerous images taken from multiple angles by calculation; however, SfM has reduced reconstruction accuracy if the plant surface does not have a characteristic pattern or shape. In the case of relatively large plants, such as agricultural plants, SfM is expected to be sufficient for three-dimensional reconstruction. However, in the case of *Arabidopsis*, which is small and has limited characteristic textures and structures, the visual volume intersection method might be more suitable. Therefore, it is difficult to adequately reproduce planar and thinner structures, such as leaves, even with the visual volume intersection method. Although our proposed method was sufficient for three-dimensional reconstruction of the inflorescence stem and branches, improvements such as changing the camera angle or major changes in the algorithm for three-dimensional reconstruction would be necessary when applying the method to plants with leaves.

For multiple-angle imaging, we chose an imaging setup that rotates the plant and not the camera (**Fig. 2**). This eliminates the need to build a setup to control camera motion, which makes it inexpensive and space saving. Our imaging system fits into a 1.5 m^2 space and, therefore, can be set up in small available space in a laboratory or environmentally controlled room. However, there are some limitations due to the plant rotation. First, only potted plants can be analyzed. When applied to field plants, substantial changes in the imaging system are required. Second, the plant shakes when it rotates, which reduces reconstruction accuracy. We observed vibrations of the plants if the plants were too tall or the rotation speed was too fast. If the plant shakes, we recommend attaching a support to the plant or slowing down the rotation speed. Interestingly, it was previously reported that some kinds of cell wall-related mutants showed a phenotype in which the inflorescence stem easily shakes (Nakata et al. 2018). Therefore, preliminary rotation experiments using the plants of interest are needed to optimize the rotation speed. In addition, wind and floor vibrations can also shake the plants; therefore, depending on the location, measures should be taken against these factors. Third, we cannot deny the possibility that rotation can affect plant development and growth. In the time-lapse observation example shown in this study, the plants were mounted on the rotating table twice for 72 hours and rotated for only around 1 minute each time (**Fig. 4**). Therefore, we believe that the negative effects of rotation were extremely limited. However, if you want to shorten the imaging intervals to improve the temporal resolution, it will be necessary to evaluate the effect of rotation on plant growth by comparing plants without rotation as a control.

We also successfully measured the angles and curvatures of the lateral branches from the reconstructed three-dimensional images via skeletonization (**Fig. 5A**, **B**; **Supplementary Fig. S2**). These measurements are useful for refining *Arabidopsis* architecture phenotyping because the three-dimensional measures more accurately reflect actual plant architectures than two-dimensional approximations using an image taken from a single angle that is subjectively chosen by the human researchers. In fact, we were able to quantitatively evaluate the phenotype of *lazy1* mutants with these features (**Figs. 5**, **6**; **Supplementary Figs. S2, S3**). Of course, angle and curvature are just examples of measurements of three-dimensional plant architecture, and additional morphological features might be added depending on the phenotype. The combination of our proposed three-dimensional measurements and molecular genetics of *Arabidopsis* is expected to dramatically improve our understanding of the molecular mechanisms that regulate plant architecture.

In conclusion, we developed a three-dimensional scanning system for digital archiving and quantitative evaluation of *Arabidopsis* architectures. Our system requires no special equipment, is space efficient and inexpensive and can be easily adopted in laboratories that specialize in plant molecular

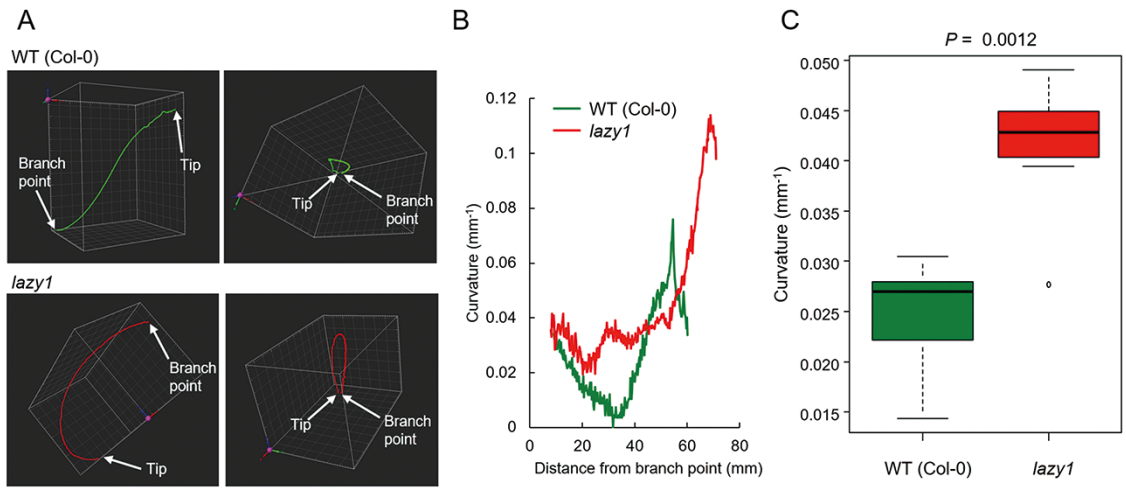

Fig. 6 Measurements of lateral branch curvatures. (A) Three-dimensional images of binarized lateral branches of the WT Col-0 (42 days old) (top, green) and *lazy1* mutant (48 days old) plants (bottom, red). Images from different viewpoints are shown. The branch points and tips are indicated by arrows. (B) Spatial distributions of the curvatures of the branch in (A). (C) Comparison of the mean curvatures in WT (Col-0) and *lazy1* mutant plants. Note that the branch curvature in the *lazy1* mutants was significantly higher than that in the WT plants. Statistical significance was determined by Mann–Whitney U-tests ($P = 0.0012$). We analyzed seven (WT) and eight branches (*lazy1* mutant) from three WT and three *lazy1* mutant plants.

biology. Using our proposed method in combination with *Arabidopsis* molecular genetics would promote our understanding of molecular mechanisms that regulate three- and four-dimensional plant architectures.

Materials and Methods

Plant materials and growth conditions

WT (Col-0) and *lazy1* mutant *A. thaliana* (Taniguchi et al. 2017) were used. The seeds were sown in soil (Jiffy-7, Sakata Seed Corp., Yokohama, Japan) and incubated in a growth chamber at 23.5°C with a 16 hours light/8 hours dark cycle using an 86.2 μmol m^{-2} s^{-1} light-emitting diode for plant growth (Plantflec; LH-241PFP-S, NK System, Tokyo, Japan) for approximately 10 days. Then, the plant was replaced in the vermiculite in a pot and incubated in the same growth chamber under the same conditions. The plant was watered with 0.5 g L^{-1} Hyponex solution (Hyponex Japan, Osaka, Japan). Just before the start of movie acquisition (0 hours), the cauline leaves near the branch points were cut off with precision scissors; then, the rosette leaves were covered with black cloth. After movie acquisition, the black cloth was taken off and the plant was placed back in the growth chamber until the second movie was made.

Calibration target

For the calibration target design, we licensed and modified the pattern by Baumberg et al. (2005) (**Fig. 2C**, **Supplementary Material S1**) (Elsevier license number: 5026340638206). We defined the center-of-gravity coordinates of the markers as $P_i^j\left(x_i^j, y_i^j\right)$, where $i = 1, 2, \ldots, 15$ and $j = 0, 1, 2, 3$ (in order of distance from the origin) is the cluster number and marker number, respectively. In the case of the first cluster ($i = 1$), the center-of-gravity coordinates of the markers were defined as $P_1^j\left(x_1^j, y_1^j\right) = P_1^j(r - j \cdot dr, 0)$, where r is the X-coordinate of the first cluster marker nearest the origin ($r = x_1^0$); therefore, the X-axis was defined as the vector from the center to the makers in the first cluster. In the cases of the second and latter clusters ($i = 2, 3, \ldots, 15$), the center-of-gravity coordinates of the markers were defined as $P_i^j\left(x_i^j, y_i^j\right) = P_i^j\left(x_1^j \cos\theta - y_1^j \sin\theta, x_1^j \sin\theta + y_1^j \cos\theta\right)$, where θ is the angle between the X-axis and the vector from the center to the makers in each cluster. Here, θ was defined as $\theta = \varphi \cdot (i - 1)$, where φ is the angle between the X-axis and the vector from the center to the markers in the second cluster. We generated the target pattern file and printed it to the label seal paper with an inkjet printer, setting the parameters as follows: $r = 94.146\,[mm]$, $dr = 13.149\,[mm]$, $\varphi = 24°$ (Supplementary Material). The printed seal was carefully placed on a 1.5 cm-thick acrylic plate with a center hole.

Image acquisition

The image acquisition system consisted of a digital single-lens reflex camera (EOS Kiss X10, Canon Inc., Tokyo, Japan) equipped with a single-focus lens (EF28IS, Canon Inc.), rotator (RT-5, TAITEC, Saitama, Japan), calibration target for camera posture estimation, illumination and a background blackout curtain. The approximate dimensions of the entire system were 1.5 m wide × 1.5 m long × 1.5 m high. First, a pot with an *A. thaliana* plant was placed into the center hole of the calibration target, which was attached to the rotating plate of the rotator. The rotating plate was rotated at a speed of approximately 2.5 rpm. The rotating object was captured for approximately 1 minute in movie mode using a fixed-point camera (30 fps, 1,080 × 1,920 pixels, 1 pixel = ~0.25 mm) that was tilted −12° and set approximately 70 cm from the plant. The frames of the movie were extracted as the captured images for analysis. The frame extraction ratio can be arbitrarily changed; however, in this study, one frame was extracted for every four frames. Therefore, around 450 frames were extracted from approximately 1 minute of video (30 fps × 60 seconds = 1,800 frames) and used for three-dimensional reconstruction.

Three-dimensional reconstruction software construction and performance

We developed a script for three-dimensional reconstruction based on the visual volume intersection method (Tsai 1987, Laurentini 1994, Kutulakos and Seitz 2000, Cheung et al. 2005). This script was implemented in the Python language (https://www.python.org/) and is executable in Windows and macOS. The script is only for academic purposes and freely available at our website (https://ie.u-ryukyu.ac.jp/~kunita/download_plant3d.html). The representative list of the parameters used in this study is shown in **Supplementary Table S1**. For volume rendering, we used the software Imaris (Bitplane, Belfast, UK). In our framework, we first estimated the camera matrix that represented the

positional relationship between the plant and camera. Second, we generated silhouette images. Third, we calculated visual volume using the camera matrix and a silhouette image. Finally, we calculated the intersection region in which there was intersected visual volume among frames and defined the region as the plant presence region. The specific procedures are described as follows.

Camera matrix estimation

Based on the pinhole camera model, the relationship between the three-dimensional world coordinates of the object $\boldsymbol{W} = [\boldsymbol{X}, \boldsymbol{Y}, \boldsymbol{Z}]$ and the image coordinates of the captured image $\boldsymbol{x_i} = (\boldsymbol{x_i}, \boldsymbol{y_i})$ are described as $\boldsymbol{x_i} = \boldsymbol{PW}$, where $\boldsymbol{P}$ is the camera matrix (Tsai 1987). The camera matrix $\boldsymbol{P}$ is the inner product $\boldsymbol{K}[\boldsymbol{R}, \boldsymbol{t}]$ of the intrinsic parameter $\boldsymbol{K}$ and the extrinsic parameters $[\boldsymbol{R}, \boldsymbol{t}]$ of the camera. Intrinsic parameters represent geometric optical properties of the camera, such as focal length, optical center and lens distortion. Extrinsic parameters represent the location of the camera in the world coordinate system with the components of a rotation matrix $\boldsymbol{R}$ and a translation vector $\boldsymbol{t}$. Calibration target markers with known world coordinates were used to estimate the camera matrix $\boldsymbol{P}$. The camera matrix $\boldsymbol{P}$ was estimated by the world coordinates that corresponded to the image coordinates of the markers in the captured images. Specifically, the intrinsic parameter $\boldsymbol{K}$ was obtained by Zhang's method (Zhang 2000), and the camera matrix $\boldsymbol{P}$, which included the external parameter $[\boldsymbol{R}, \boldsymbol{t}]$, was estimated using the intrinsic parameter $\boldsymbol{K}$ by iterative optimization calculation using the Levenberg–Marquardt method (Marquardt 1963). Because these markers are known in the world coordinate system, we used a modified calibration target proposed by Baumberg et al. (2005) (**Fig. 2C**, **Supplementary Material S1**). The drawing plane of the calibration target was defined as the X–Y plane of the world coordinate system $\boldsymbol{W}$ ($Z = 0$). The average coordinates of the markers were defined as the origin $\boldsymbol{W} = [0, 0, 0]$. The X-axis was defined as the vector from the origin to the center of the reference marker when one of the 60 markers was used as the reference marker. The Y-axis was defined as a vector orthogonal to the X-axis passing through the origin in the X–Y plane. The scale of the world coordinate system was determined based on the distance between the origin and center of the reference marker. The world coordinates of each marker were calculated from the relative positions of the reference marker and each marker. The image coordinates of the markers were determined by detecting the markers in the captured images.

Silhouette image generation

To obtain the silhouette images, which are binary images that represent the existence areas of the target plants, we first saved the movie frames as 24-bit Red-Green-Blue (RGB) color images. Then, the green channel images were binarized by Otsu's method.

Intersection region calculation

The intersection regions of the visual volume were determined by the space carving method algorithm. The three-dimensional reconstruction space was represented as voxels with a side length of 0.2 mm. The center coordinates of each voxel were reprojected to the silhouette image plane, and the number of frames in which the reprojected coordinates were inside the silhouette was defined as the crossover numbers. We also introduced the cross ratio (CR, %) of the visual volume intersection to determine the region that allows for some loss of visual volume caused by camera noise or plant shaking. The CR is defined as the percentage of images that are judged to be the crossover area of the target object out of the total number of analyzed images (CR corresponds to the gray areas in **Fig. 1B**). In this study, we used 70–90% of the CR for thresholding.

Three-dimensional printing of the sphere model for accuracy verification

The sphere model was printed by a light-curing 3D printer (LCD Photon, Shenzhen Anycubic Technology Co., Ltd., Shenzhen, China), with the following parameters: XY resolution, 0.0047 mm; Z-axis accuracy, 0.00125 mm; layer XY resolution, 0.0047 mm; layer Z-axis accuracy, 0.00125 mm; layer thickness, 0.01–0.20 mm (**Supplementary Fig. S1A**).

Branch angle and curvature estimation

Based on the reconstructed three-dimensional images, we first performed skeletonization of the plant architecture using Lee's algorithm (Lee et al. 1994). To define the three-dimensional filamentous structures, we adopted a 26-connection method. The basal and tip end points with one voxel connection in the stem were manually specified, and the shortest path connecting these end points was defined as the primary inflorescence stem. Additionally, the paths from the voxels with more than two voxel connections (branch points) in the stem to the unspecified end points were defined as lateral branches. The end points and branch points in the stem were represented as $N_{ms}(i)$, with basal end points as $i = 0$, branch points as $i = 1, \ldots, N-1$ and tip end points as $i = N$.

We then calculated the angle between the inflorescence stem and lateral branch $\theta(i,j) = \cos^{-1}(\boldsymbol{V}_{ms} \cdot \boldsymbol{V}_{br}(j) / (\boldsymbol{V}_{ms}\boldsymbol{V}_{br}(j)))$, where i is the number of branch points described above and j is the voxel number of the branch segment. $\boldsymbol{V}_{ms}$ is the stem vector, which is the vector from $N_{ms}(i)$ to $N_{ms}(i+1)$. $\boldsymbol{V}_{br}(j)$ is the branch vector, which is the vector from $N_{ms}(i)$ to the jth voxel in the branch.

We also calculated the branch curvature $R(i,j) = 1/r(i,j)$, where $r(i,j)$ is the radius of the circle passing through three points S, T, U on the ith branch. Here, $r(i,j) = \overrightarrow{CS} = \overrightarrow{CT} = \overrightarrow{CU}$, where C is the center coordinate of the circle. Given that O is the origin of the coordinate space where the circle exists, $\vec{n} \cdot \overrightarrow{CS} = 0$ (Equation 1). Moreover, because P is the midpoint of side ST of a triangle with three points S, T, U, $\overrightarrow{ST} \cdot \overrightarrow{CP} = 0$ (Equation 2) because the line passing through P and the circle center coordinate C is the perpendicular bisector of side ST. Similarly, when Q is the midpoint of edge SU, $\overrightarrow{SU} \cdot \overrightarrow{CQ} = 0$ (Equation 3). By solving linear equations 1, 2 and 3, the center coordinate C was found and used to calculate the curvature $R(i,j) = 1/r(i,j)$.

Supplementary Data

Supplementary data are available at PCP online.

Funding

Japan Society for the Promotion of Science KAKENHI to T.H. (18H05492 and 20H03289) and M.T.M. (18H05488).

Disclosures

No conflicts of interest declared.

Acknowledgements

We thank Ms. Hitomi Okada (Kumamoto University) for her support in plant maintenance and image acquisition. We thank Mallory Eckstut, PhD, from Edanz Group (https://en-author-services.edanz.com/ac), for editing a draft of this manuscript and helping to draft the abstract.

Data Availability

The scripts for three-dimensional reconstruction, skeletonization and curvature measurement underlying this article are available in our website at https://ie.u-ryukyu.ac.jp/~kunita/download_plant3d.html.

References

Baumberg, A., Lyons, A. and Taylor, R. (2005) 3D SOM—a commercial software solution to 3D scanning. *Graph. Models* 67: 476–495.

Cheung, K.M., Baker, S. and Kanade, T. (2005) Shape-from-silhouette across time part I: theory and algorithms. *Int. J. Comput. Vis.* 62: 221–247.

Datta, A., Kim, J.S. and Kanade, T. (2009) Accurate camera calibration using iterative refinement of control points. *In* 2009 IEEE 12th International Conference on Computer Vision Workshops, ICCV Workshops. pp. 1201–1208. IEEE, Piscataway.

Golbach, F., Kootstra, G., Damjanovic, S., Otten, G. and Van De Zedde, R. (2016) Validation of plant part measurements using a 3D reconstruction method suitable for high-throughput seedling phenotyping. *Mach. Vis. Appl.* 27: 663–680.

Gülci, S. (2019) The determination of some stand parameters using SfM-based spatial 3D point cloud in forestry studies: an analysis of data production in pure coniferous young forest stands. *Environ. Monit. Assess.* 191: 495.

Hill, J.L., Jr. and Hollender, C.A. (2019) Branching out: new insights into the genetic regulation of shoot architecture in trees. *Curr. Opin. Plant Biol.* 47: 73–80.

Hongo, S., Sato, K., Yokoyama, R. and Nishitani, K. (2012) Demethylesterification of the primary wall by PECTIN METHYLESTERASE35 provides mechanical support to the *Arabidopsis* stem. *Plant Cell* 24: 2624–2634.

Kutulakos, K.N. and Seitz, S.M. (2000) A theory of shape by space carving. *Int. J. Comput. Vis.* 38: 199–218.

Laurentini, A. (1994) The visual hull concept for silhouette-based image understanding. *IEEE Trans. Pattern Anal. Mach. Intell.* 16: 150–162.

Lee, T.C., Kashyap, R.L. and Chu, C.N. (1994) Building skeleton models via 3-D medial surface/axis thinning algorithms. *Comput. Vis. Graph. Image Process.* 56: 462–478.

Marquardt, D.W. (1963) An algorithm for least-squares estimation of nonlinear parameters. *J. Soc. Ind. Appl. Math.* 11: 431–441.

Mitsuda, N., Iwase, A., Yamamoto, H., Yoshida, M., Seki, M., Shinozaki, K., et al. (2007) NAC transcription factors, NST1 and NST3, are key regulators of the formation of secondary walls in woody tissues of *Arabidopsis*. *Plant Cell* 19: 270–280.

Nakamasu, A. and Higaki, T. (2019) Theoretical models for branch formation in plants. *J. Plant Res.* 132: 325–333.

Nakata, M.T., Takahara, M., Sakamoto, S., Yoshida, K. and Mitsuda, N. (2018) High-throughput analysis of Arabidopsis stem vibrations to identify mutants with altered mechanical properties. *Front. Plant Sci.* 9: 780.

Okamoto, K., Ueda, H., Shimada, T., Tamura, K., Kato, T., Tasaka, M., et al. (2015) Regulation of organ straightening and plant posture by an actin–myosin XI cytoskeleton. *Nat. Plants* 1: 15031.

Omasa, K., Hosoi, F. and Konishi, A. (2007) 3D lidar imaging for detecting and understanding plant responses and canopy structure. *J. Exp. Bot.* 58: 881–898.

Paproki, A., Sirault, X., Berry, S., Furbank, R. and Fripp, J. (2012) A novel mesh processing based technique for 3D plant analysis. *BMC Plant Biol.* 12: 63.

Paturkar, A., Gupta, G.S. and Bailey, D. (2020) Non-destructive and cost-effective 3D plant growth monitoring system in outdoor conditions. *Multimed. Tools App.* 79: 34955–34971.

Qiu, Q., Sun, N., Bai, H., Wang, N., Fan, Z., Wang, Y., et al. (2019) Field-based high-throughput phenotyping for maize plant using 3D LiDAR point cloud generated with a 'Phenomobile'. *Front. Plant Sci.* 10: 554.

Scharr, H., Briese, C., Embgenbroich, P., Fischbach, A., Fiorani, F. and Müller-Linow, M. (2017) Fast high resolution volume carving for 3D plant shoot reconstruction. *Front. Plant Sci.* 8: 1680.

Sussex, I.M. and Kerk, N.M. (2001) The evolution of plant architecture. *Curr. Opin. Plant Biol.* 4: 33–37.

Takenaka, Y., Watanabe, Y., Schuetz, M., Unda, F., Hill, J.L., Phookaew, P., et al. (2018) Patterned deposition of xylan and lignin is independent from that of the secondary wall cellulose of *Arabidopsis* xylem vessels. *Plant Cell* 30: 2663–2676.

Taniguchi, M., Furutani, M., Nishimura, T., Nakamura, M., Fushita, T., Iijima, K., et al. (2017) The *Arabidopsis* LAZY1 family plays a key role in gravity signaling within statocytes and in branch angle control of roots and shoots. *Plant Cell* 29: 1984–1999.

Tsai, R.Y. (1987) A versatile camera calibration technique for high-accuracy 3D machine vision metrology using off-the-shelf TV cameras and lenses. *IEEE J. Robot. Autom.* 3: 323–344.

Wang, Y. and Jiao, Y. (2018) Axillary meristem initiation—a way to branch out. *Curr. Opin. Plant Biol.* 41: 61–66.

Zhang, Z. (2000) A flexible new technique for camera calibration. *IEEE Trans. Pattern Anal. Mach. Intell.* 22: 1330–1334.